Effect of Ni, Bi and Se on the tetrahedrite formation

António Pereira Gonçalves, Elsa Branco Lopes, Benjamin Villeroy, Judith Monnier, Claude Godart, Bertrand Lenoir

RSC Advances

PAPER

View Article Online
View Journal | View Issue

Cite this: *RSC Adv.*, 2016, **6**, 102359

Effect of Ni, Bi and Se on the tetrahedrite formation

António Pereira Gonçalves,*[a] Elsa Branco Lopes,[a] Benjamin Villeroy,[b] Judith Monnier,[b] Claude Godart[b] and Bertrand Lenoir[c]

Received 26th August 2016
Accepted 20th October 2016

DOI: 10.1039/c6ra21482g

www.rsc.org/advances

Materials based on $Cu_{12}Sb_4S_{13}$ tetrahedrites have been seen in recent years as promising materials for thermoelectric applications. However, the effect of small amounts of additional elements (used to tune the electrical transport properties) on the formation of the phases was not investigated. In this work we present such study, by means of powder X-ray diffraction, scanning electron microscopy complemented with energy-dispersive spectroscopy, and differential scanning calorimetry, using the Taguchi method to design the experiments. The effect of Ni, Bi and Se (i) in the volume percentage of tetrahedrite, (ii) in the temperature at which the Class III (tetrahedrite + chalcostibite + antimony → skinnerite) reaction occurs and (iii) in the final melting temperature of $Cu_{12-x}Ni_xSb_{4-y}Bi_yS_{13-z}Se_z$ materials rapidly cooled from 950 °C was investigated. Se was observed to have a strong positive influence on the formation of tetrahedrite, while Ni and Bi were seen to promote the decrease of its volume percentage. A decrease of the Class III reaction and final melting temperatures was also observed after the introduction of Se, with Ni inducing the increase of the reaction and the decrease of the melting temperatures and Bi having only minor effects. The analysis of the microstructures indicate that high Ni concentrations lead to the first solidification of the NiS phase, while in the other compositions the (tetrahedrite/skinnerite) phase or mixtures of phases is first formed.

1. Introduction

Thermoelectric systems are devices that directly convert heat into electricity (*via* the Seebeck effect) and, *vice versa*, heat or cool through the passage of an electrical current (*via* the Peltier effect). They have a huge potential to recover part of the waste heat released by human activity, being seen as promising components for a more sustainable world. However, the present commercial thermoelectric devices have small efficiencies, which are directly related to the low performance of the thermoelectric materials that depends only on their basic electrical and thermal transport properties.[1] Moreover, actual commercial thermoelectric materials contain expensive and/or toxic elements and, consequently, the discovery of new ones is critical for a more general use of thermoelectricity.

Recently, tetrahedrite-based materials were considered promising for thermoelectric applications.[2–12] Tetrahedrites are wide-spread copper sulfosalt minerals, with $Cu_{10}M_2Sb_4S_{13}$ (M = Cu, Mn, Fe, Co, Ni, Zn) general formula, that crystallize in the cubic $Cu_{12}Sb_4S_{13}$-type structure.[13,14] They are rather environment friendly materials since are mainly formed by the non-expensive copper and sulfur elements.[15] Though, tetrahedrite does not melt congruently, participating in several reactions, mostly to give Cu_3SbS_3 (skinnerite),[16,17] which is stable until its congruent melting point (~605 °C). The lower temperature reaction is the Class III (tetrahedrite + $CuSbS_2$ (chalcostibite) + antimony → skinnerite), at 359 °C, which consumes tetrahedrite and forms skinnerite, with comparable elemental formula. Furthermore, other reactions involving tetrahedrite take place between 436 °C and 543 °C (ref. 16 and 17) and complex decompositions can occur when extra elements are present.[18,19] As a result, for the preparation of single phase tetrahedrite materials solid state reactions are normally used after casting, with long-term annealing procedures. A large starting volume percentage of tetrahedrite in the as-cast substance is expected to favor the preparation of the single phase material. However, only limited information on the tetrahedrite formation from the undoped liquid phase exists.[16–19]

During the last years, alternative, cheap, rapid and scalable methods for tetrahedrite preparation have been developed, in particular using solvothermal synthesis, mechanical alloying and glass crystallization.[20–22] In these preparations extra elements were added, either to tune the electrical properties of the materials or to act as vitrifying and nucleating agents. Nevertheless, information on the effect of extra elements in the formation and stabilization of tetrahedrite-based thermoelectric materials is scarce: up to the authors best knowledge, only one article deals with this subject (a study on the effect of small amounts of iron in the stability region of tetrahedrite and phase

[a]*C²TN, Instituto Superior Técnico, Universidade de Lisboa, Departamento de Engenharia e Ciências Nucleares, Estrada Nacional 10, 2695-066 Bobadela LRS, Portugal. E-mail: apg@ctn.tecnico.ulisboa.pt; Tel: +351 219946182*

[b]*Université Paris Est, ICMPE (Institut de Chimie et des Matériaux Paris-Est, UMR 7182), CNRS, UPEC, F-94320 THIAIS, France*

[c]*Institut Jean Lamour, UMR 7198, CNRS, Université de Lorraine, Nancy, France*

relations).[23] Some results were also recently reported, but for samples prepared by solid state reaction[24] and mechanical milling.[25] No other information on the evolution of the reactions and melting temperatures with doping exists.

In order to partially fill such gaps, here we present a study of the effect of nickel, bismuth and selenium in the volume percentage of tetrahedrite phases, in the temperature at which the Class III reaction occurs and in the final melting temperature of the $Cu_{12-x}Ni_xSb_{4-y}Bi_yS_{13-z}Se_z$ materials rapidly cooled from 950 °C. Nickel, bismuth and selenium were chosen due to their use in previously reported materials with good thermoelectric characteristics.[4,12,22,24] To carry out these studies efficiently the Taguchi method was applied, using data obtained from powder X-ray diffraction (PXRD), differential scanning calorimetry (DSC) and scanning electron microscopy (SEM), complemented with energy-dispersive spectroscopy (EDS). The analysis of the solidification microstructures of selected samples, together with the corresponding DSC data, were also used to obtain information on the formation of the (tetrahedrite/skinnerite) phase or mixtures of phases, $CuSbS_2$, NiS and Cu_3SbS_4.

2. Methods and materials

2.1. Application of the Taguchi method

The Taguchi method is an easy-to-use statistical technique to make robust design of experiments.[26] It employs a limited number of specific orthogonal arrays, each of which is utilized in a number of particular experimental situations in order to organize the parameters affecting a certain process and the levels at which they should be varied. The arrays stipulate the minimal number of experiments necessary to determine which factors most affect the process, allowing an independent evaluation of each factor. In the evaluation of results, three different types of quality characteristics, "bigger is better", "smaller is better" and "nominal is best" are classified in the Taguchi method.

The Taguchi method has been recently implemented with success in several Materials Science studies.[27–31] Studies as distinct as the optimization of the fabrication of TiO_2–Nb_2O_5–Al_2O_3 mixed oxide nanotube arrays on Ti–6Al–7Nb,[27] the design of multicomponent ferrospinels for high-temperature purposes,[28] the densification of ZrB_2-based composites by reactive hot pressing with changes in ZrO_2/SiC ratio and sintering conditions,[29] the bond strength optimization of Ti/Cu/Ti clad composites produced by roll-bonding,[30] or the synthesis of minimal-size ZnO nanoparticles through sol–gel method[31] were recently made using the Taguchi method. In these works, L-9 and L-32 orthogonal arrays[26] were used, allowing a strong decrease in the number of experiences needed to determine the optimal conditions.

2.1.1. Design of experiments. The identified general factors that can affect the tetrahedrite concentration are the initial composition, the thermal treatment, the ampoule (sample container), the nature of the atmosphere and the quantity of material. This study is focused on the effect of the initial composition, in particular of the Ni, Bi and Se elements in the tetrahedrite formation. Therefore, the effect of parameters like the quantity of material, type of atmosphere, quartz ampoule diameter, quartz wall thickness, thermal treatment conditions (heating speed(s), maximum heating temperature(s), time at the plateau(s) and cooling procedure(s)) was not studied and, consequently, they were kept constant in all experiments. The selected input factors were three, the substitution of (i) Ni for Cu, (ii) Bi for Sb and (iii) Se for S. Considering the general formula $Cu_{12-x}Ni_xSb_{4-y}Bi_yS_{13-z}Se_z$, the (i), (ii) and (iii) input factors are represented by x, y and z, respectively. The number of levels for each one was also three, as nonlinear effects can be present. The input factors and their selected levers are summarized in Table 1. For three three-level input factors a standard Taguchi L-9 orthogonal array to design experiments was chosen.[26]

Table 1 Selected input factors and their respective levels in the actual experimental design

Input factor	Level 1	Level 2	Level 3
x	0	0.5	1
y	0	0.2	0.4
z	0	1	3

The Taguchi L-9 orthogonal array used in the experimental layout, after assigning the input factor values, is presented in Table 2. In the last column are shown the desired compositions after considering the substitutions. According to the L-9 orthogonal array, a total of nine independent experiments are needed to perform this study. It must be noted that in the L-9 orthogonal array all factors are considered independent. In fact, this design is not suitable to investigate the interactions between the different factors in three three-level input factors. It would be possible only if much larger orthogonal arrays were used, which would lead to a great increase in the number of experiments, decreasing the advantage of the Taguchi method. Therefore, and to simplify, all factors were considered independent and the L-9 array was used.

Since zero cannot be used in the signal-to-noise ratios calculation, a content of 0.1 volume percentage was considered for the phases not detected. A maximum amount of tetrahedrite phase is wanted. For this reason, in the evaluation of results, we used "bigger is better" for this phase and "smaller is better" for the others.

Table 2 Taguchi L-9 orthogonal array used for the present experimental layout, after assigning the input factor values (the last column indicates the desired/target composition)

Experiment no.	x	y	z	Composition
1	0	0	0	$Cu_{12}Sb_4S_{13}$
2	0	0.2	1	$Cu_{12}Sb_{3.8}Bi_{0.2}S_{12}Se$
3	0	0.4	3	$Cu_{12}Sb_{3.6}Bi_{0.4}S_{10}Se_3$
4	0.5	0	1	$Cu_{11.5}Ni_{0.5}Sb_4S_{12}Se$
5	0.5	0.2	3	$Cu_{11.5}Ni_{0.5}Sb_{3.8}Bi_{0.2}S_{10}Se_3$
6	0.5	0.4	0	$Cu_{11.5}Ni_{0.5}Sb_{3.6}Bi_{0.4}S_{13}$
7	1	0	3	$Cu_{11}NiSb_4S_{10}Se_3$
8	1	0.2	0	$Cu_{11}NiSb_{3.8}Bi_{0.2}S_{13}$
9	1	0.4	1	$Cu_{11}NiSb_{3.6}Bi_{0.4}S_{12}Se$

2.2. Experimental procedure

The polycrystalline samples, with ~1 g mass each, were prepared by reacting the elements (Cu, ≥99.999%, Sigma-Aldrich; Ni, 99.97%, Johnson Matthey; Sb, 99.999%, Ventron; Bi, 99.997%, Alfa Aesar; S, 99.9%, Alfa Aesar; Se, 99.99+%, Sigma-Aldrich) inside a quartz ampoule of 10 mm outer diameter and 1 mm wall thickness sealed under vacuum. An excess, up to 4 mol%, of the chalcogenide elements (S, Se) was considered to compensate eventual evaporation losses. The temperature of the elemental mixture was raised from room temperature to 950 °C (when only one liquid phase is present) with an average heating speed of 3 °C min^{-1}, kept at that temperature for 60 minutes and quenched into cold water.

The thermodynamic behavior of the samples was studied from room temperature up to 600 °C, under argon atmosphere, with a flux of 50 cm^3 min^{-1}, and using a TA Instruments Q100 differential scanning calorimeter. The DSC measurements were made with a heating rate of 10 °C min^{-1} in a ~5 to 35 mg weighed sample.

A representative part of each sample was manually powdered and characterized by PXRD. Low-noise Si single crystal X-ray diffraction sample holders were used in a PANalytical X'Pert Pro powder diffractometer (Cu Kα-radiation) with Bragg-Brentano geometry. Step-scanning mode X-ray diffraction patterns were taken in the 15–60° 2θ region with the $\theta/2\theta$ configuration, a step scan of 0.01° and a counting time per step of 15 s. The theoretical powder patterns were calculated with the help of the Powder-Cell package.[32] The lattice parameters and unit cell volumes were obtained by least-squares fitting using the UnitCell program.[33] Rietveld refinements were made using the FullProf software,[34] with Pseudo-Voigt profile shape function and manually introduced background. As the number of electrons are similar in copper and nickel, the copper positions were always considered totally filled, whereas no constrains were made for the antimony and sulfur occupations. All thermal displacement parameters were fixed.

Scanning electron microscopy (SEM) was used to characterize the microstructure of the samples. The SEM observations were made on pieces of samples embedded in resin, polished using SiC paper and diamond paste down to 1 μm, and with a thin layer of gold deposited on the surface. A JEOL JSM-7001F field emission gun scattering electron microscope, equipped for energy-dispersive spectroscopy (EDS) with a light element detector was used in the microstructural characterizations. At least three EDS point analysis were obtained for each phase. The image analysis of the electron micrographs was made with the help of ImageJ 1.46r software.[35]

For each independent experiment the volume percentage of the different phases existing in the samples was determined by three separated times using Rietveld refinements, while for the melting temperatures determination only one DSC measurement was made for each sample.

3. Results and discussions

The average values of the volume percentage of the different phases that exist in the samples, the corresponding signal-to-

Table 3 Summarized results of the volume percentage of the different phases existing in the samples, reaction (T_r) and melting (T_m) temperatures[a]

Experiment no.	Sample	Target composition	Composition	$Cu_{12}Sb_4S_{13}$ vol%		Cu_3SbS_3 vol%		$CuSbS_2$ vol%		NiS vol%		Cu_3SbS_4 vol%		$Cu_{12}Sb_4S_{13}$ S/N (larger is better)	T_r (°C)	T_m (°C)
				XR	IA	XR	IA	XR	IA	XR	IA	XR	IA			
1	A1	$Cu_{12}Sb_4S_{13}$	$Cu_{12}Sb_{4.007}S_{13.1}$	32	*84*	55	*84*	2	5	—	—	11	11	30.1	360	>600
2	A2	$Cu_{12}Sb_{3.8}Bi_{0.2}S_{12}Se$	$Cu_{12}Sb_{3.789}Bi_{0.192}S_{11.986}Se_{1.071}$	98	82	—	—	2	18	—	—	—	—	39.8	300	583
3	A3	$Cu_{12}Sb_{3.6}Bi_{0.4}S_{10}Se_3$	$Cu_{12}\ Sb_{3.621}Bi_{0.41}S_{10.026}Se_{3.212}$	90	*92*	8	*92*	2	8	—	—	—	—	39.1	250	553
4	A4	$Cu_{11.5}Ni_{0.5}Sb_4S_{12}Se$	$Cu_{11.5}Ni_{0.532}Sb_{3.988}S_{12.272}Se_{1.238}$	97	97	—	—	3	3	—	—	—	—	39.7	320	584
5	A5	$Cu_{11.5}Ni_{0.5}Sb_{3.8}Bi_{0.2}S_{10}Se_3$	$Cu_{11.5}Ni_{0.507}Sb_{3.784}Bi_{0.208}S_{10.012}Se_{3.077}$	48	28	41	64	11	8	—	—	—	—	33.6	310	550
6	A6	$Cu_{11.5}Ni_{0.5}Sb_{3.6}Bi_{0.4}S_{13}$	$Cu_{11.5}Ni_{0.504}Sb_{3.581}Bi_{0.401}S_{13.317}$	47	57	53	43	—	—	—	—	—	—	33.4	370	585
7	A7	$Cu_{11}NiSb_4S_{10}Se_3$	$Cu_{11}Ni_{1.003}Sb_{3.994}S_{9.994}Se_{3.129}$	83	75	—	—	12	16	5	9	—	—	38.2	310	561
8	A8	$Cu_{11}NiSb_{3.8}Bi_{0.2}S_{13}$	$Cu_{11}Ni_{1.01}Sb_{3.78}Bi_{0.206}S_{13.16}$	20	46	61	41	4	4	15	9	—	—	26.0	370	587
9	A9	$Cu_{11}NiSb_{3.6}Bi_{0.4}S_{12}Se$	$Cu_{11}Ni_{0.975}Sb_{3.593}Bi_{0.399}S_{11.996}Se_{1.013}$	6	*85*	76	*85*	4	4	14	11	—	—	15.6	370	575

[a] XR, X-ray diffraction; IA, image analysis. Italics numbers represent the sum of the vol% of tetrahedrite and skinnerite phases (see main text).

noise ratios and the Class III reaction and final melting temperatures are summarized in Table 3. Due to the similarity between the compositions of some tetrahedrite and skinnerite phases it was not possible to use image analysis for the calculation of volume percentages in three of the samples, being only possible to determine the volume percentage of their sum. Therefore, just the results of volume percentages obtained from Rietveld refinements were used in the Taguchi calculations. However, as can be seen in Table 3, the results obtained from both methods (Rietveld refinement and image analysis) are roughly in agreement. All these data allowed the application of the Taguchi method to study the influence of nickel, bismuth and selenium in the volume percentage of the phases and in the Class III reaction and final melting temperatures of the $Cu_{12-x}Ni_xSb_{4-y}Bi_yS_{13-z}Se_z$ materials, which are presented below.

Additional information was also obtained by the analysis of the solidification microstructures. However, as noted before, the lack of contrast between tetrahedrite and skinnerite did not permit the proper separation of these two phases in the microstructures of three samples. For that reason, the analysis was made for the (tetrahedrite/skinnerite) phase or mixture of phases, $CuSbS_2$, NiS and Cu_3SbS_4, which provided relevant information on their formation during solidification.

3.1. Effect of composition on the volume of the phases

Fig. 1 presents the X-ray diffraction patterns of the $Cu_{12-x}Ni_xSb_{4-y}Bi_yS_{13-z}Se_z$ samples, together with simulations for the tetrahedrite (T) and skinnerite (S) phases. The representative microstructures of the $Cu_{12-x}Ni_xSb_{4-y}Bi_yS_{13-z}Se_z$ materials, namely, of the A1, A3, A4, A6 and A7 samples, are shown in Fig. 2. A simple observation of the diffractograms indicates that all samples are mainly formed by these two phases, which was confirmed by the Rietveld refinements (Table 3). EDS composition analyses (Table 4) are in agreement with the X-ray diffraction data, with the image analysis pointing to a total volume percentage of these two phases higher than 80% in all samples (Fig. 2 and Table 3). The Grand Average of Performance (the average of all trial results) for tetrahedrite, skinnerite, chalcostibite ($CuSbS_2$), millerite (NiS) and famatinite (Cu_3SbS_4) weight percentage is 57.7, 32.7, 4.3, 3.8 and 1.2, respectively. These results clearly confirm the preponderance of tetrahedrite and skinnerite in the samples. However, depending on the initial composition there is a predominance of one of the phases, when compared with the volume of the other.

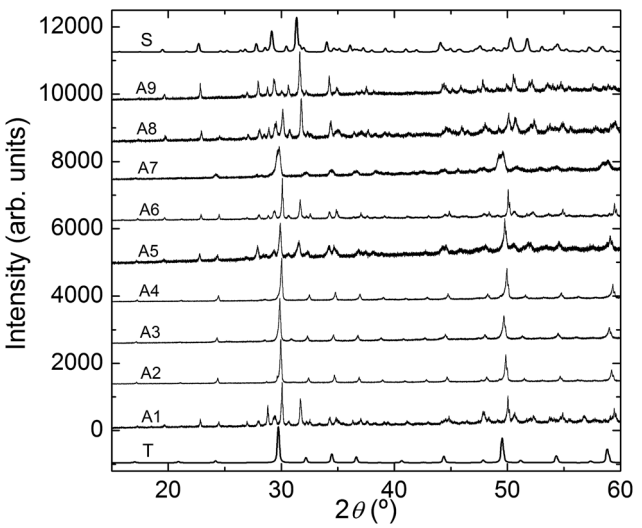

Fig. 1 X-ray diffraction patterns of $Cu_{12-x}Ni_xSb_{4-y}Bi_yS_{13-z}Se_z$ samples. The simulations of X-ray diffraction patterns for the tetrahedrite (T-line) and skinnerite (S-line) type structures are included for reference.

It is possible to have an idea on the factor-level contribution for the formation of the different phases from average values. The average factor-level effects (average values for each level) on the volume percentage of the different phases are presented in Table 5 and those for tetrahedrite and skinnerite are plotted in Fig. 3. It can be seen that the increase of nickel content has a detrimental influence on the tetrahedrite formation. However, its effect seems to be small for low nickel contents, strongly increasing with the increase of this element in the material. On the contrary, nickel linearly promotes the formation of skinnerite and leads to the development of a millerite-based phase, while only a slight effect on the remaining phases is observed. Similarly to nickel, bismuth has also a negative effect on the tetrahedrite formation, but on a linear way. It also favors the development of skinnerite and millerite, having a small effect on the other phases. The effect of selenium strongly contrasts with those of the other two elements: small amounts of it greatly increase the quantity of tetrahedrite and decreases the volume percentage of skinnerite. A slight increase of the chalcostibite-based phase and a negligible effect on the remaining ones is also observed.

Albeit the analysis of the average values alone can give important information on the influence of different factors, those based on signal-to-noise (S/N) ratios can be used to analyze the results in a better way, as they give information not only on the average values, but also on the variation around those values. When the maximum is the ideal value it is desired to use the "bigger is better" model, with S/N being given by

$$\frac{S}{N} = -10 \log_{10}\left[\frac{1}{n}\sum\left(\frac{1}{Y_i}\right)^2\right] \quad (1)$$

where n represents the number of obtained results for each set of input factor values and Y_i represents each individual result at those conditions. If the minimum is wanted should be used the "smaller is better" model and in this case S/N is given by

$$\frac{S}{N} = -10 \log_{10}\left[\frac{1}{n}\sum Y_i^2\right] \quad (2)$$

In the present analysis "bigger is better" was used for the tetrahedrite-based phases, while "smaller is better" was used for the others as mentioned previously.

The factor average effects on the volume percentage of the different phases, based on the S/N ratios, are presented in Table 6 and shown in Fig. 4. The factor that has a positive

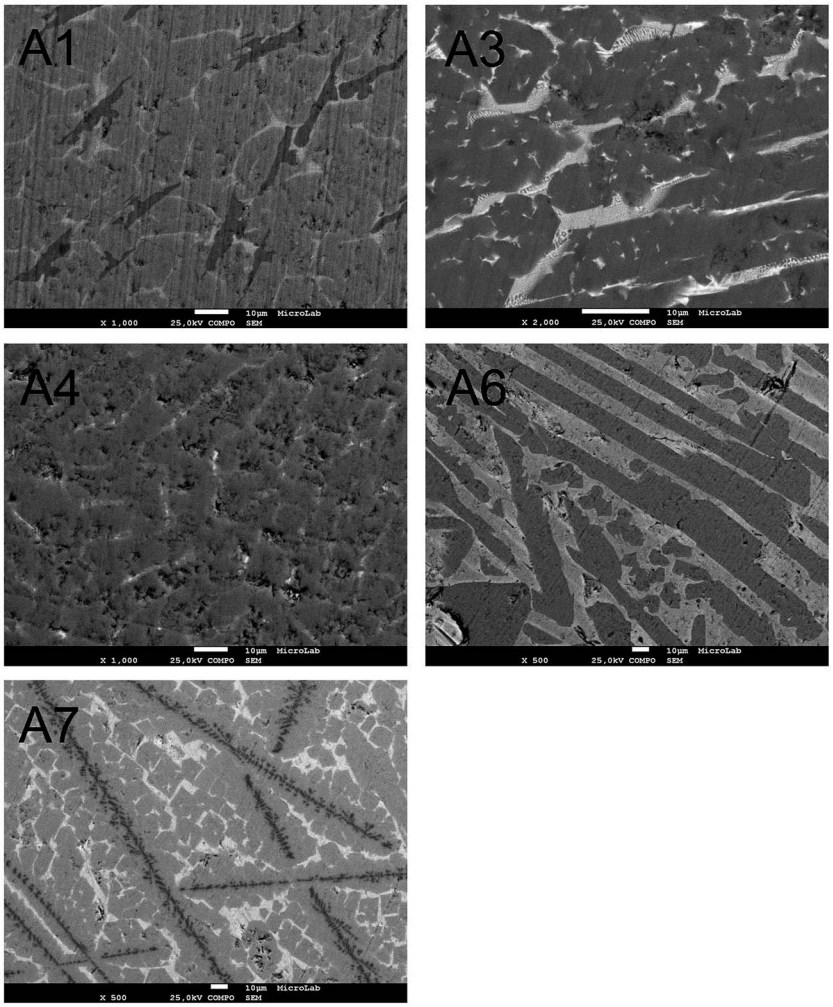

Fig. 2 Representative microstructures of the $Cu_{12-x}Ni_xSb_{4-y}Bi_yS_{13-z}Se_z$ samples. A1: grey-(tetrahedrite/skinnerite) phase or mixture of phases, light grey-chalcostibite ($CuSbS_2$), dark grey-famatinite (Cu_3SbS_4); A3 and A4: grey-(tetrahedrite/skinnerite) phase or mixture of phases, light grey-chalcostibite ($CuSbS_2$); A6: grey-tetrahedrite, light grey-skinnerite; A7: dark grey-NiS, grey-tetrahedrite, light grey-chalcostibite ($CuSbS_2$).

impact on the tetrahedrite formation is the selenium content in the sample, being desirable to have the z value close to 3. The nickel substitution for copper can go up to $x = 0.5$ with negligible effects on the tetrahedrite concentration, but higher values induce the formation of other phases, in particular of the chalcostibite. The results also indicate that bismuth has a negative effect on the tetrahedrite formation, which agrees with the EDS data and previous studies that showed that this element does not enter into the tetrahedrite structure,[22] and promotes the development of the skinnerite and chalcostibite phases. The contribution of bismuth for the tetrahedrite formation is always negative, increasing with the concentration increase, and therefore only minor amounts of bismuth can be inside the sample before the appearance of visible effects.

3.2. Effect of composition on the Class III reaction and final melting temperatures

DSC curves obtained for the different samples are shown in Fig. 5. The temperature at which the Class III reaction (tetrahedrite + chalcostibite + antimony → skinnerite) occurs and the final melting temperature of the $Cu_{12-x}Ni_xSb_{4-y}Bi_yS_{13-z}Se_z$ materials, that should mostly correspond to the skinnerite congruent melting, are summarized in Table 3. Since only one DSC measurement was performed for each sample, only the analysis of average values was made in the Taguchi calculations.

3.2.1. Class III reaction temperatures. The (tetrahedrite + chalcostibite + antimony → skinnerite) Class III reaction was reported to occur at 359 °C in materials with the $\sim Cu_{12}Sb_4S_{13}$ composition.[16] In the present study, the DSC measurement of an unsubstituted sample with the same type of composition (A1) shows an anomaly at ~360 °C, which was ascribed to this reaction and confirms the previous published results.

The average effects of the different parameters and levels on the reaction temperatures for all samples are presented in Table 7. The addition of each one of the three elements produces a very different effect: nickel causes a large increase of the reaction temperature; bismuth makes no significant change; and selenium induces a great temperature decrease. These results are in agreement with the (scarce) previous reported data, where tetrahedrite was observed to be the major

Table 4 Results from average EDS analysis for the phases in the $Cu_{12-x}Ni_xSb_{4-y}Bi_yS_{13-z}Se_z$ samples

			Composition EDS/at%					
Sample	Nominal composition	Phase	Cu	Ni	Sb	Bi	S	Se
A1	$Cu_{12}Sb_{4.007}S_{13.1}$	$Cu_{12}Sb_4S_{13}/Cu_3SbS_3$	40(1)	—	15(1)	—	45(1)	—
		$CuSbS_2$	29(2)	—	22(2)	—	49(1)	—
		Cu_3SbS_4	36.9(1)	—	12.6(3)	—	50.5(3)	—
A2	$Cu_{12}Sb_{3.789}Bi_{0.192}S_{11.986}Se_{1.071}$	$Cu_{12}Sb_4S_{13}$	41.2(2)	—	13.5(2)	0	43.3(2)	2.1(1)
		$CuSbS_2$	35(6)	—	10(4)	8(3)	32(3)	15(4)
A3	$Cu_{12}Sb_{3.621}Bi_{0.41}S_{10.026}Se_{3.212}$	$Cu_{12}Sb_4S_{13}/Cu_3SbS_3$	41.8(3)	—	13.3(3)	0	38.5(2)	6.4(1)
		$CuSbS_2$	30(4)	—	10(2)	13(3)	16(2)	30(4)
A4	$Cu_{11.5}Ni_{0.532}Sb_{3.988}S_{12.272}Se_{1.238}$	$Cu_{12}Sb_4S_{13}$	39.1(4)	2.3(2)	14.0(4)	—	42.9(1)	1.8(2)
		$CuSbS_2$	32(4)	0	20(2)	—	26(2)	22(2)
A5	$Cu_{11.5}Ni_{0.507}Sb_{3.784}Bi_{0.208}S_{10.012}Se_{3.077}$	$Cu_{12}Sb_4S_{13}$	41(2)	2(1)	13(1)	0	36(3)	7(2)
		Cu_3SbS_3	41(1)	1(1)	14(1)	0	31(1)	12(1)
		$CuSbS_2$	38(8)	0	9(2)	9(3)	12(2)	32(4)
A6	$Cu_{11.5}Ni_{0.504}Sb_{3.581}Bi_{0.401}S_{13.317}$	$Cu_{12}Sb_4S_{13}$	39.1(2)	3.1(2)	13.6(2)	0	44.2(3)	—
		Cu_3SbS_3	43(1)	0	11(1)	3(1)	43(1)	—
A7	$Cu_{11}Ni_{1.003}Sb_{3.994}S_{9.994}Se_{3.129}$	$Cu_{12}Sb_4S_{13}$	43(1)	1(1)	14(1)	—	36(1)	6(1)
		$CuSbS_2$	32(3)	0	22(2)	—	23(2)	23(2)
		NiS	8(2)	38(3)	2(1)	—	43(3)	9(1)
A8	$Cu_{11}Ni_{1.01}Sb_{3.78}Bi_{0.206}S_{13.16}$	$Cu_{12}Sb_4S_{13}$	38(3)	4(2)	13(1)	0	45(1)	—
		Cu_3SbS_3	42(1)	1(1)	14(1)	1(1)	43(1)	—
		$CuSbS_2$	33(3)	1(1)	17(2)	2(1)	47(2)	—
		NiS	12(2)	32(2)	5(1)	0	51(1)	—
A9	$Cu_{11}Ni_{0.975}Sb_{3.593}Bi_{0.399}S_{11.996}Se_{1.013}$	$Cu_{12}Sb_4S_{13}/Cu_3SbS_3$	40(3)	2(2)	14(1)	2(1)	44(2)	2(1)
		$CuSbS_2$	34(5)	0	14(3)	8(3)	30(4)	17(3)
		NiS	10(2)	35(3)	3(2)	0	42(3)	9(2)

phase in selenium containing 12Cu:3.6Sb:0.4Bi:10S:3Se glassy samples treated below 250 °C, while those treated above this temperature were mainly constituted by skinnerite.[22]

3.2.2. Melting temperatures. The final melting temperatures of the $Cu_{12-x}Ni_xSb_{4-y}Bi_yS_{13-z}Se_z$ materials are presented in Table 3. These temperatures should correspond to the skinnerite congruent melting, as tetrahedrite transforms into this phase at high temperatures. For the sample A1 (with the $Cu_{12}Sb_4S_{13}$ composition) that has its final melting above 600 °C, a temperature of 605 °C was considered. This temperature corresponds to the congruent, unsubstituted, skinnerite congruent melting temperature (~605 °C (ref. 16)), as tetrahedrite participates in several reactions, between 359 °C and 543 °C that result in this phase.[16,17]

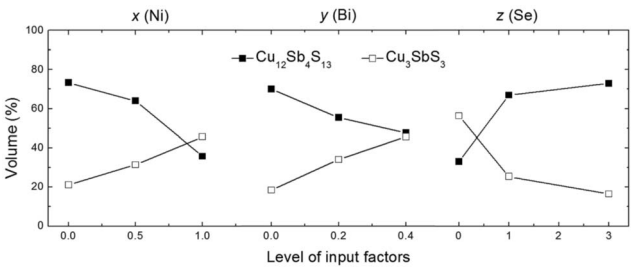

Fig. 3 Average effects of the studied factor-levels (*x*, *y*, *z*) on the volume percentage of tetrahedrite and skinnerite.

Table 8 presents the average effects of the different parameters and levels on the melting temperatures of the samples. The introduction of nickel, bismuth and selenium always

Table 5 Average effects of factor levels on the volume percentage of the different phases[a]

		Properties				
Process parameter	Levels	$Cu_{12}Sb_4S_{13}$	Cu_3SbS_3	$CuSbS_2$	NiS	Cu_3SbS_4
$(Ni)_x$	0	73	21	2	0	4
	0.5	64	31	5	0	0
	1	36	46	6	11	0
$(Bi)_y$	0	70	18	5	2	4
	0.2	55	34	6	5	0
	0.4	48	46	2	5	0
$(Se)_z$	0	33	56	2	5	4
	1	67	25	3	5	0
	3	73	16	8	2	0

[a] Grand average of performance for: tetrah. – 57.7; skin. – 32.7; chal. – 4.3; mill. – 3.8 fam. – 1.2.

Table 6 Factor average effects on the volume percentage of the different phases, based on the S/N ratios

		Properties				
Process parameter	Levels	$Cu_{12}Sb_4S_{13}$	Cu_3SbS_3	$CuSbS_2$	NiS	Cu_3SbS_4
$(Ni)_x$	0	36	−11	−6	20	8
	0.5	36	−16	−3	20	20
	1	27	−18	−16	−20	20
$(Bi)_y$	0	36	2	−13	9	8
	0.2	33	−16	−12	6	20
	0.4	29	−30	1	6	20
$(Se)_z$	0	30	−35	1	6	8
	1	32	1	−9	6	20
	3	37	−10	−16	9	20

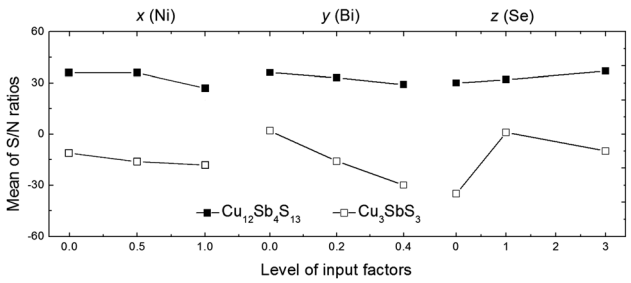

Fig. 4 Factor average effects for the mean S/N ratios of the volume percentage of tetrahedrite ("bigger is better") and skinnerite ("smaller is better"), as a function of the studied factor-levels (*x*, *y*, *z*).

decrease the melting temperature. However, the effect of the first two elements is small when compared with selenium. A decrease of ~10 °C when changing from the first to the third level is observed for nickel and bismuth, while in the case of selenium a change of ~40 °C is seen, pointing this factor as the most influent on the melting temperature. Previous DSC studies on $Cu_{12}Sb_4S_{13}$ and $Cu_{10.4}Ni_{1.6}Sb_4S_{13}$ are consistent with the present results, confirming the decrease of the final melting temperature when nickel exists,[24] but our study emphasize the predominant action of Se on the melting temperature.

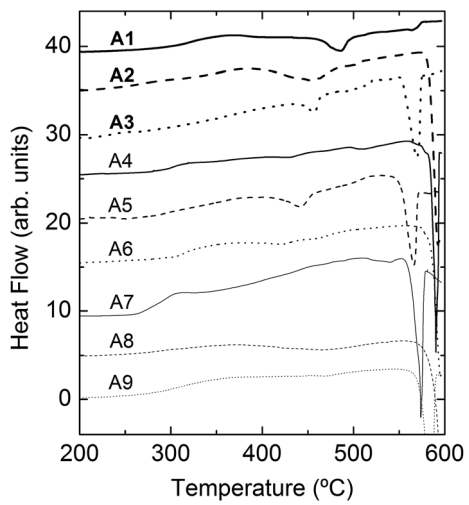

Fig. 5 DSC curves obtained for the $Cu_{12-x}Ni_xSb_{4-y}Bi_yS_{13-z}Se_z$ samples.

3.3. Microstructures

The cooling rates associated to quenching into cold water (estimated to be close to 10^2 °C s^{-1}) do not allow the proper solid state diffusion necessary to reach equilibrium, which promotes the presence of liquid below *de equilibrium* solidification temperatures. Therefore, the microstructures can evidence extended solidification paths that give significant information on the monovariant lines and type of ternary reactions. However, precautions must be taken, as these cooling rates can also induce the formation of metastable phases and/or suppress the nucleation of equilibrium phases. Slower cooling rates are expected to promote equilibrium and, consequently, the phases more stable at lower temperatures, which in the present case are the tetrahedrite ones.

The representative microstructures of the $Cu_{12-x}Ni_xSb_{4-y}Bi_yS_{13-z}Se_z$ materials, namely, of the A1, A3, A4, A6 and A7 samples, are shown in Fig. 2. EDS results of all alloys are summarized in Table 4 and DSC curves are presented in Fig. 5.

The A1 sample has three clear regions, a (tetrahedrite/skinnerite) phase or mixture of phases, in grey, chalcostibite ($CuSbS_2$), in light grey and famatinite (Cu_3SbS_4), in dark grey. The (tetrahedrite/skinnerite) seems to be the first to solidify, as famatinite is generally surrounded by chalcostibite, the phase that is produced from the last liquid. The introduction of bismuth, selenium and small amounts of nickel leads to the disappearance of famatinite, with the last liquid always solidifying into a region rich in the chalcostibite phase. In samples A3 and A5 the liquid composition reaches a monovariant line with eutectic nature: l_1: L → (tetrahedrite/skinnerite) + chalcostibite. The solidification of the chalcostibite phase and/or {(tetrahedrite/skinnerite) + chalcostibite} eutectic occurs between 400 °C and 500 °C, as indicated by the peaks seen in the DSC measurements. The endothermic broad peak that is observed between 555 °C and 570 °C in the DSC curve of sample A1 can be attributed to the decomposition reaction of Class I (tetrahedrite → skinnerite + $Cu_{2-x}S$ + famatinite), albeit it is slightly above the reported values.[16,24] This difference is most probably due to kinetic reasons, as in the DSC measurement

Table 7 Average effects of factor levels on the (tetrahedrite + chalcostibite + antimony → skinnerite) reaction temperature

Process parameter	Levels	Reaction temperature, T_r (°C), average
$(Ni)_x$	0	303.3
	0.5	333.3
	1	350.0
$(Bi)_y$	0	330.0
	0.2	326.7
	0.4	330.0
$(Se)_z$	0	366.7
	1	330.0
	3	290.0

Table 8 Average effects of factor levels on the final melting temperatures of the samples

Process parameter	Levels	Melting temperature, T_m (°C), average
$(Ni)_x$	0	580.3
	0.5	573.0
	1	574.3
$(Bi)_y$	0	583.3
	0.2	573.3
	0.4	571.0
$(Se)_z$	0	592.3
	1	580.7
	3	554.7

there is a continuous heating and the tetrahedrite decomposition rate is limited by solid state diffusion.[36]

A4 has minor amounts of chalcostibite and only a small anomaly that can be related with its melting in the 400–500 °C range exists. This sample contains a large quantity of pores, which most probably are connected with the sulfur release due to the high temperatures involved. Another possibility is their relation with the (tetrahedrite → skinnerite + $Cu_{2-x}S$ + famatinite) Class I reaction that occurs at 500–520 °C, temperatures lower than in the unsubstituted material, as is evidenced by an irregularity in the DSC curve. In a similar way, samples A2 and A3 also have an anomaly at these temperatures, but unfortunately it was not possible to systematically study the effect of composition on this Class I reaction, as the other samples do not show a clear anomaly that could be related with it. However, these results seem to indicate that the substitutions decrease this reaction temperature.

In contrast with the previous samples, in A6 there is an unambiguous distinction between the tetrahedrite and skinnerite phases. This is related with their specific compositions, in particular to their content of nickel and bismuth (Table 4). Interestingly, tetrahedrite is the first phase to crystallize, showing grains with flat surfaces and a well defined morphology.

Samples A7, A8 and A9 have black NiS dendrites solidifying first, followed by the grey (tetrahedrite/skinnerite) phase or mixture of phases and, finally, chalcostibite, in light grey, crystallizing from the last liquid. From these three samples, a broad peak between 515 °C and 550 °C is only observed in the DSC curve of A7 that should be related with the melting of chalcostibite. It should be noted that, from these three samples, A7 is the only that has a higher concentration of this phase.

4. Conclusions

The Tagushi method was applied to study the effect of nickel, bismuth and selenium in the tetrahedrite volume percentage on $Cu_{12-x}Ni_xSb_{4-y}Bi_yS_{13-z}Se_z$, in the Class III reaction and in the melting temperatures of those samples and on their microstructure. Selenium was found to have the higher impact on the tetrahedrite formation, as well as on the reaction and melting temperature decrease. On the contrary, bismuth and nickel do not promote the tetrahedrite formation, but they have different effects on the transformation reactions, as nickel increase the Class III reaction temperature without significant effect on melting temperature, whereas bismuth does not have major effect on none of these two temperatures. The microstructure derived from these effects were also investigated.

These studies are part of a broader project that has as main objective to predict the amount of tetrahedrite phases on samples prepared under different conditions.

Acknowledgements

This work was partially supported by the Portuguese Foundation for Science and Technology (FCT), Portugal, through the contracts UID/Multi/04349/2013 and POCI-01-0145-FEDER-016674. We would also like to acknowledge the support given by the ANR project "PROGELEC", Verres Thermo-Générateurs "VTG".

References

1 C. Wood, *Rep. Prog. Phys.*, 1988, **51**, 459–539.
2 K. Suekuni, K. Tsuruta, T. Ariga and M. Koyano, *Appl. Phys. Express*, 2012, **5**, 051201.
3 X. Lu, D. T. Morelli, Y. Xia, F. Zhou, V. Ozolins, H. Chi, X. Zhou and C. Uher, *Adv. Energy Mater.*, 2013, **3**, 342–348.
4 K. Suekuni, K. Tsuruta, M. Kunii, H. Nishiate, E. Nishibori, S. Maki, M. Ohta, A. Yamamoto and M. Koyano, *J. Appl. Phys.*, 2013, **113**, 043712.
5 X. Lu and D. T. Morelli, *Phys. Chem. Chem. Phys.*, 2013, **15**, 5762–5766.
6 X. Lu and D. Morelli, *J. Electron. Mater.*, 2014, **43**, 1983–1987.
7 J. Heo, G. Laurita, S. Muir, M. A. Subramanian and D. A. Keszler, *Chem. Mater.*, 2014, **26**, 2047–2051.
8 R. Chetty, P. D. S. Kumar, G. Rogl, P. Rogl, E. Bauer, H. Michor, S. Suwas, S. Puchegger, G. Giesterg and R. C. Mallik, *Phys. Chem. Chem. Phys.*, 2015, **17**, 1716–1727.
9 X. Lu, D. T. Morelli, Y. Xia and V. Ozolins, *Chem. Mater.*, 2015, **27**, 408–413.
10 Y. Bouyrie, C. Candolfi, V. Ohorodniichuk, B. Malaman, A. Dauscher, J. Tobola and B. Lenoir, *J. Mater. Chem. C*, 2015, **3**, 10476–10487.

11 Y. Bouyrie, S. Sassi, C. Candolfi, J.-B. Vaney, A. Dauscher and B. Lenoir, *Dalton Trans.*, 2016, 7294–7302.
12 X. Lu, D. T. Morelli, Y. Wang, W. Lai, Y. Xia and V. Ozolins, *Chem. Mater.*, 2016, **28**, 1781–1786.
13 L. Pauling and E. W. Neuman, *Z. Kristallogr.*, 1934, **88**, 54–62.
14 B. J. Wuensch, *Z. Kristallogr.*, 1964, **119**, 437–453.
15 U.S. Geological Survey: Commodity Statistics Information, U.S. Department of Interior, http://minerals.usgs.gov/minerals/pubs/commodity/.
16 B. J. Skinner, F. D. Luce and E. Makovicky, *Econ. Geol.*, 1972, **67**, 924.
17 M. H. Braga, J. A. Ferreira, C. Lopes and L. F. Malheiros, *Mater. Sci. Forum*, 2008, **587–588**, 435–439.
18 T. A. Ibragimov and R. A. Isakova, *Kompleksn. Ispol'z. Miner. Syr'ya*, 1989, **1**, 25.
19 T. A. Ibragimov and R. A. Isakova, *Kompleksn. Ispol'z. Miner. Syr'ya*, 1989, **2**, 45.
20 D. J. James, X. Lu, D. T. Morelli and S. L. Brock, *ACS Appl. Mater. Interfaces*, 2015, **7**, 23623.
21 T. Barbier, S. Rollin-Martinet, P. Lemoine, F. Gascoin, A. Kaltzoglou, P. Vaqueiro, A. V. Powell and E. Guilmeau, *J. Am. Ceram. Soc.*, 2016, **99**, 51–56.
22 A. P. Gonçalves, E. B. Lopes, J. Monnier, J. Bourgon, J. B. Vaney, A. Piarristeguy, A. Pradel, B. Lenoir, G. Delaizir, M. F. C. Pereira, E. Alleno and C. Godart, *J. Alloys Compd.*, 2016, **664**, 209–217.
23 K. Tatsuka and N. Morimoto, *Am. Mineral.*, 1977, **62**, 1101–1109.
24 T. Barbier, P. Lemoine, S. Gascoin, O. I. Lebedev, A. Kaltzoglou, P. Vaqueiro, A. V. Powell, R. I. Smith and E. Guilmeau, *J. Alloys Compd.*, 2015, **634**, 253–262.
25 S. Harish, D. Sivaprahasam, M. Battabyal and R. Gopalan, *J. Alloys Compd.*, 2016, **667**, 323–328.
26 R. K. Roy, *Design of experiments using the Taguchi approach*, John Wiley & Sons, Inc., New York, 2001.
27 A. R. Rafieerad, A. R. Bushroa, B. Nasiri-Tabrizi, J. Vadivelu, S. Baradaran, E. Zalnezhad and A. Amiri, *RSC Adv.*, 2016, **6**, 10527–10540.
28 N. M. Ferreira, M. C. Ferro, S. M. Mikhalev, F. M. Costa, J. R. Frade and A. V. Kovalevsky, *RSC Adv.*, 2016, **6**, 32540–32548.
29 N. P. Vafa, M. S. Asl, M. J. Zamharir and M. G. Kakroudi, *Ceram. Int.*, 2015, **41**, 8388–8396.
30 M. Hosseini and H. D. Manesh, *Mater. Des.*, 2015, **81**, 122–132.
31 Y. T. Chung, M. M. Ba-Abbad, A. W. Mohammad, N. H. H. Hairom and A. Benamor, *Mater. Des.*, 2015, **87**, 780–787.
32 G. Nolze and W. Kraus, *Powder Cell for Windows (Version 2.3)*, Federal Institute for Materials Research and Testing, Berlin, 1999.
33 T. J. B. Holland and S. A. T. Redfern, *Mineral. Mag.*, 1997, **61**, 65–77.
34 J. Rodriguez-Carvajal and T. Roisnel, FullProf.98 and WinPLOTR: New Windows 95/NT Applications for Diffraction Commission for Powder Diffraction, International Union for Crystallography, (May–August) Summer, 1998. Newsletter No. 20.
35 C. A. Schneider, W. S. Rasband and K. W. Eliceiri, *Nat. Methods*, 2012, **9**, 671.
36 P. Baláz, J. Briancin and L. Turcániová, *Thermochim. Acta*, 1995, **249**, 375–381.